SECURITY INFORMATION

[redacted]

[redacted]

NACA

RESEARCH MEMORANDUM

for the

U, S. Army Ordnance

WIND-TUNNEL INVESTIGATION OF THE STATIC LONGITUDINAL STABILITY CHARACTERISTICS OF A 0.15-SCALE MODEL OF THE HERMES A-1E2 MISSILE AT HIGH SUBSONIC MACH NUMBERS

By William J. Alford, Jr.

Langley Aeronautical Laboratory
Langley Field, Va.

NATIONAL ADVISORY COMMITTEE
FOR AERONAUTICS

WASHINGTON
SEP 11 1952

[redacted]

NACA RM SL52I10

NATIONAL ADVISORY COMMITTEE FOR AERONAUTICS

RESEARCH MEMORANDUM

for the

U. S. Army Ordnance

WIND-TUNNEL INVESTIGATION OF THE STATIC LONGITUDINAL STABILITY CHARACTERISTICS OF A 0.15-SCALE MODEL OF THE HERMES A-1E2 MISSILE AT HIGH SUBSONIC MACH NUMBERS

By William J. Alford, Jr.

SUMMARY

The static longitudinal stability characteristics of a 0.15-scale model of the Hermes A-1E2 missile have been determined in the Langley high-speed 7- by 10-foot tunnel over a Mach number range of 0.50 to 0.98, corresponding to Reynolds numbers, based on body length, of 12.3×10^6 to 17.1×10^6. This paper presents results obtained with body alone and body-fins combinations at 0° (one set of fins vertical and the other set horizontal) and 45° angle of roll.

The results indicate that the addition of the fins to the body insures static longitudinal stability and provides essentially linear variations of the lift and pitching moment at small angles of attack throughout the Mach number range. The slopes of the lift and pitching-moment curves vary slightly with Mach number and show only small effects due to the angle of roll.

INTRODUCTION

As a result of a request made by the U. S. Army Ordnance Corps an investigation was made in the Langley high-speed 7- by 10-foot tunnel to determine the static longitudinal stability characteristics of a 0.15-scale model of the Hermes A-1E2 missile equipped with blunt trailing-edge fins. A primary reason for the investigation was to determine whether the blunt trailing-edge fins eliminated the nonlinear

variations of pitching moment at small angles of attack that are generally associated with thick airfoil sections at high subsonic speeds. (See ref. 1.)

Included in this paper are the results of body alone and body-fins combinations at 0° (one set of fins vertical and the other set horizontal) and 45° angle of roll. Lift, drag, and pitching-moment data were obtained for these configurations over a Mach number range of 0.50 to 0.98 and a tunnel-choked condition approximating a Mach number of unity, corresponding to Reynolds numbers, based on body length, of 12.3×10^6 to 17.1×10^6. The angle of attack was varied from -3° to 24°.

COEFFICIENTS AND SYMBOLS

All forces and moments are presented relative to a system of axes that has its origin at the calculated center of gravity of the model. A sketch of this axis system, showing the positive direction of forces and moments, is shown in figure 1.

C_L	lift coefficient (Lift/qS)
C_D	drag coefficient (Drag/qS)
C_m	pitching-moment coefficient (Pitching moment/qSl)
C_N	normal-force coefficient (Normal force/qS)
C_C	chord-force coefficient (Chord force/qS)
q	free-stream dynamic pressure, lb/sq ft, $\left(\frac{1}{2}\rho V^2\right)$
ρ	mass density of air, slugs/cu ft
V	free-stream velocity, ft/sec
R	Reynolds number ($\rho V l/\mu$)
M	Mach number
l	length of body, 4.23 ft
l_t	effective tail length, ft

μ	absolute viscosity, lb-sec/sq ft
S	frontal area of body, 0.146 sq ft
α	angle of attack, deg
ϕ	angle of roll (zero with one set of fins vertical and one set horizontal), deg

MODELS AND TESTS

Drawings of the model tested are shown in figure 2 and photographs of the model are shown as figure 3.

Forces and moments were measured by use of an electrical strain-gage balance located inside the model and mounted on a sting support system. Base-pressure measurements were obtained by use of a static-pressure tube located inside the model immediately ahead of the base.

These data were corrected for blockage by the method of reference 2, and the drag data were corrected to base-pressure conditions corresponding to free-stream static pressure. The center of gravity of the model was located 9.36 percent of the body length ahead of the balance center line, which necessitated a transfer to the pitching-moment data amounting to 9.36 percent of the body length. Corrections to the angle of attack due to sting deflection were calculated and found to be of the order of 1.0 percent and were neglected. Jet-boundary corrections were small and were neglected. A buoyancy correction of about 15 percent of the minimum drag, resulting from the longitudinal static-pressure gradient in the tunnel, was applied to the test results.

The data presented in this paper are results obtained with body-alone and body-fins combinations at 0° and 45° angle of roll. The Mach number range extended from 0.50 to 0.98, with some additional tests made at a tunnel-choked condition approximating a Mach number of unity. The test Reynolds numbers, based on body length, varied from 12.3×10^6 to 17.1×10^6 (fig. 4) and the angle-of-attack range extended from -3° to 24°.

RESULTS AND DISCUSSION

The data were originally obtained about the body axis (normal force and chord force) and were transferred to the system of wind axes by the following equations:

$$C_L = C_N \cos \alpha - C_C \sin \alpha$$

$$C_D = C_N \sin \alpha + C_C \cos \alpha$$

The basic data for the body-alone configuration are presented in figure 5 and the data for the complete model at 0° and 45° angle of roll are presented in figures 6 and 7, respectively. A summary of some pertinent characteristics for all configurations is presented in figure 8 and center-of-pressure locations are presented in figure 9.

Lift Characteristics

The variation of lift with angle of attack for the body-alone configuration produced typical nonlinearities (fig. 5(a)). The variations of lift with angle of attack for the body-fins combinations at 0° angle of roll (fig. 6(a)) were essentially linear in the lower angle range, with the linear range increasing slightly at the higher Mach numbers. The body-fins combinations at 45° angle of roll provided essentially linear lift variations over a slightly greater angle range than the 0° angle-of-roll configuration, with the linear range also increasing slightly with Mach number. (See fig. 7(a).) The lift variations with angle of attack for both angle-of-roll configurations were linear at the tunnel-choked condition.

Results presented in figure 8 show that the lift-curve slopes $\partial C_L/\partial \alpha$ of the body-alone configuration were small compared with those of the body-fins combinations (about 0.037 as compared with 0.145) and increased only slightly with Mach number. The lift-curve slopes of the body-fins combinations increased gradually with Mach number, and indicated that the effects of the angle of roll were negligible.

Drag Characteristics

The drag at zero lift $C_{D_{C_L=0}}$ of the body-alone configuration indicated a gradual rise with Mach number up to a Mach number of approximately 0.95 where the rate of increase was slightly greater (fig. 8). The addition of the fins caused the drag to increase about 70 percent at the lower Mach numbers and about 120 percent at the high subsonic Mach numbers. The value of $C_{D_{C_L=0}}$ for both roll configurations at the tunnel-choked condition appears to be somewhat high, probably because of the severe Mach number gradients that exist under choked conditions.

Pitching-Moment Characteristics

The pitching-moment variations for the body-alone configuration were slightly nonlinear throughout the angle-of-attack range as is shown in figure 5(c). The body-fins combination at 0° angle of roll (fig. 6(c))

showed essentially linear characteristics in the lower angle range, with the linear range remaining nearly constant throughout the Mach number range. At the higher angles of attack the body-fins combination at 0° angle of roll indicated an undesirable pitch-up tendency, which became less severe with increasing Mach number. The 45° angle-of-roll configuration (fig. 7(c)) produced linear pitching-moment variations over a slightly greater angle range than the 0° angle-of-roll configuration, with the linear range decreasing slightly at the higher Mach numbers. The pitch-up tendencies indicated by the 0° angle-of-roll configuration were reduced considerably by rotating the model through 45° of roll. It should be noted that the variations of pitching moment with angle of attack for both angle-of-roll configurations remained essentially linear at the tunnel-choked condition.

The instability of the body-alone configuration, as indicated by the slopes of the pitching-moment curves $\partial C_m/\partial\alpha$, was essentially constant throughout the Mach number range (fig. 8). The addition of the fins to the body made the model stable and provided a gradual increase in stability throughout the Mach number range, except for a Mach number of 0.91 where a slight decrease in stability was indicated. The effects of the angle of roll on the pitching-moment slopes were negligible.

The center-of-pressure location at 0° angle of attack, as indicated by $\frac{\partial C_m}{\partial\alpha}\Big/\frac{\partial C_L}{\partial\alpha}$, of the body-alone configuration was approximately 39 percent of the body length ahead of the center-of-gravity location (fig. 9) and moved rearward slightly with increasing Mach number. The center-of-pressure locations for the body-fins combinations were approximately 32 percent of the body length behind the center-of-gravity location and varied slightly with Mach number. The effect of the change in angle of roll on the center-of-pressure location was negligible. The center-of-pressure locations resulting from incremental effects of adding fins (fins plus body interference) were calculated from the following equation:

$$\frac{l_t}{l} = \frac{\left(\frac{\partial C_m}{\partial\alpha}\right)_{\text{Body + fins}} - \left(\frac{\partial C_m}{\partial\alpha}\right)_{\text{Body alone}}}{\left(\frac{\partial C_L}{\partial\alpha}\right)_{\text{Body + fins}} - \left(\frac{\partial C_L}{\partial\alpha}\right)_{\text{Body alone}}}$$

An inspection of figure 9 indicates that the effective tail center-of-pressure locations were at an average of approximately 58 percent of the body length behind the center-of-gravity location or approximately 6 percent of the body length behind the trailing edge of the fins. The indicated differences between the two angle-of-roll configurations are seen to be very small.

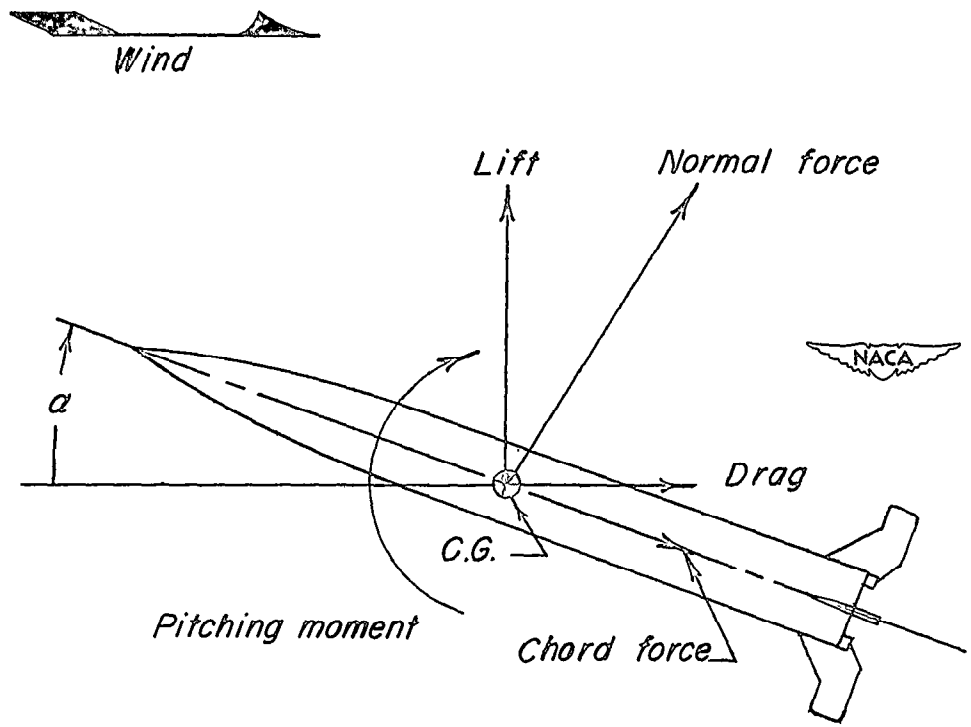

Figure 1.- Sketch of model showing system of axes and positive direction of forces and moments.

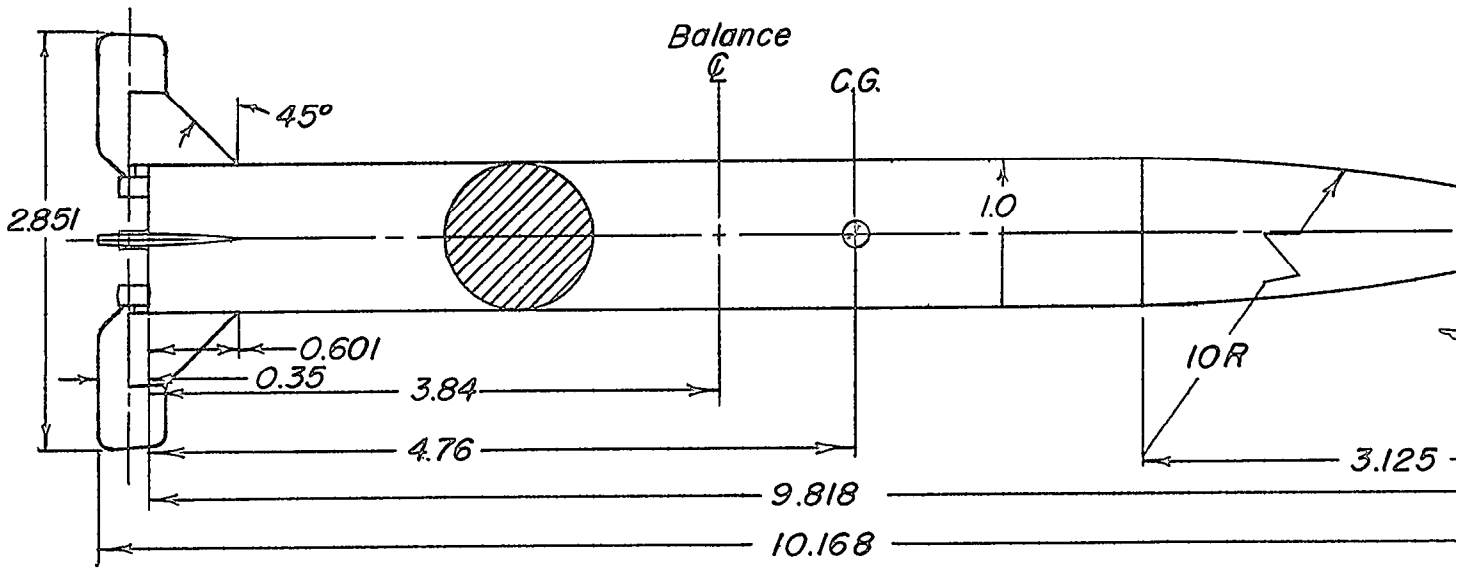

(a) General geometry.

Figure 2.- Drawing of test model. Center of gravity, 48.5 percent of body length from base of body. All dimensions in calibers (1.0 caliber is equal to 5.168 inches, model scale).

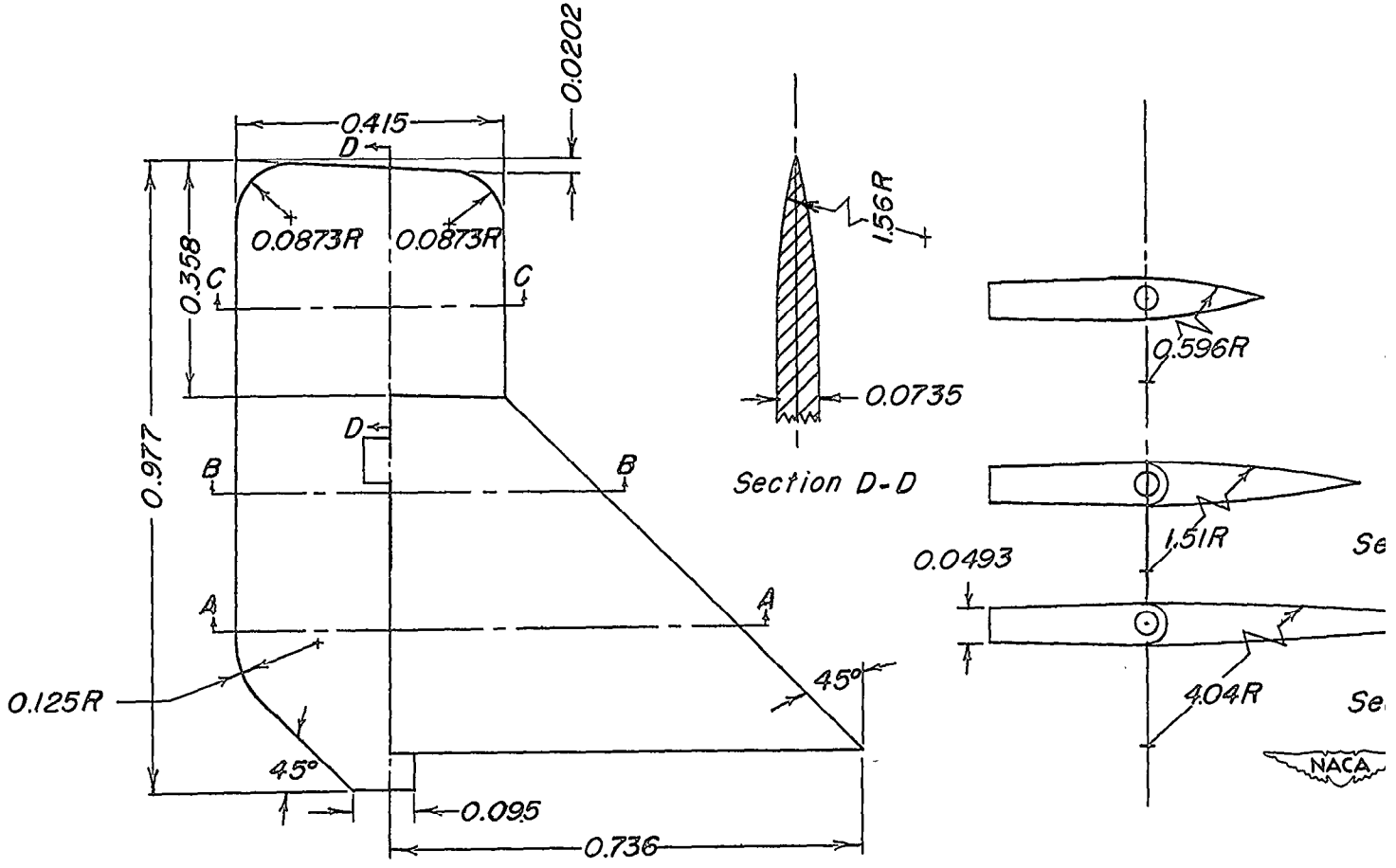

(b) Geometry of fins.

Figure 2.- Concluded. All dimensions in calibers (1.0 caliber is equal to 5.168 inches, model scale).

(a) Complete model.

Figure 3.- The 0.15-scale model of the Hermes A-1E2 missile.

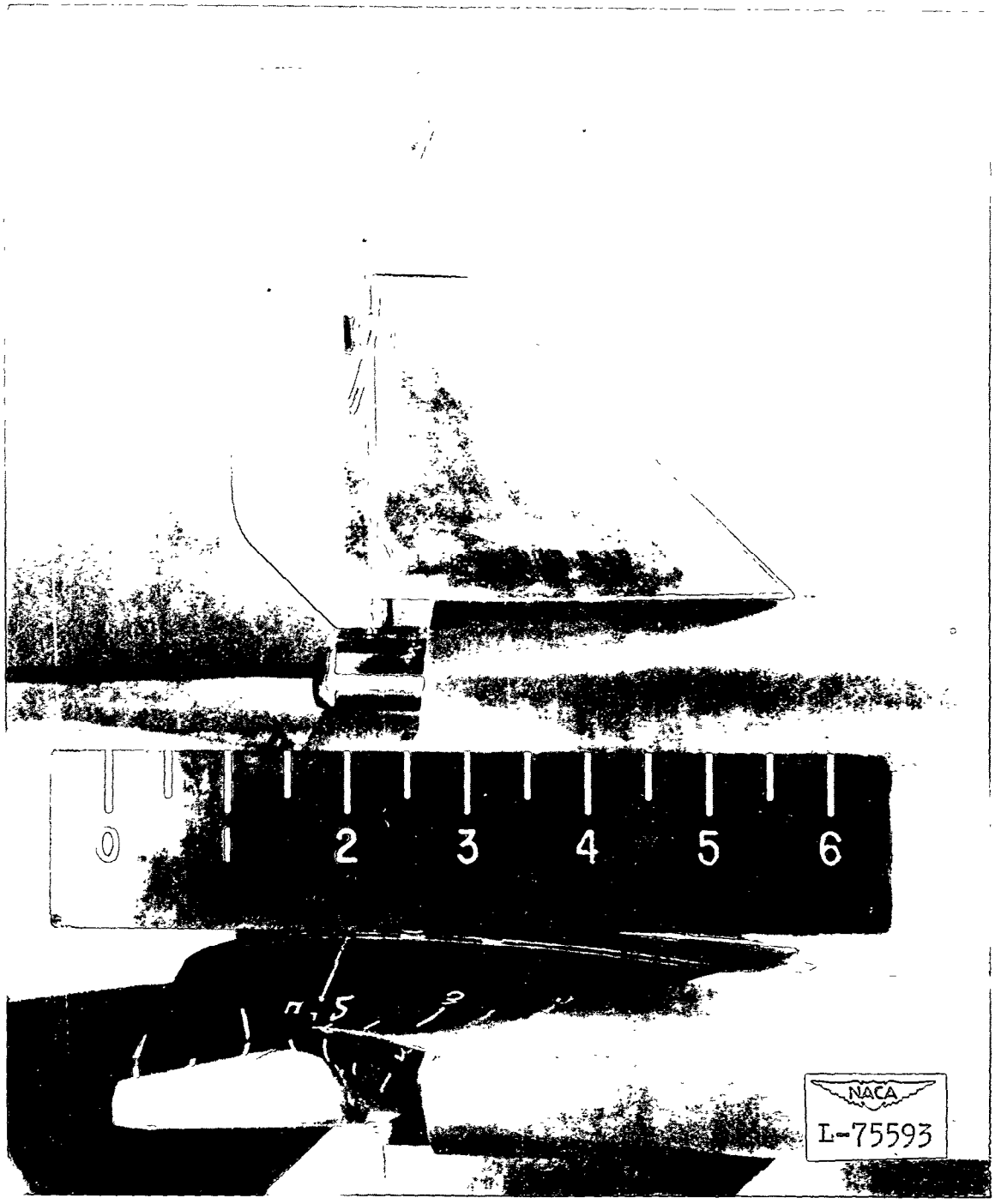

(b) Details of model fin.

Figure 3.- Concluded.

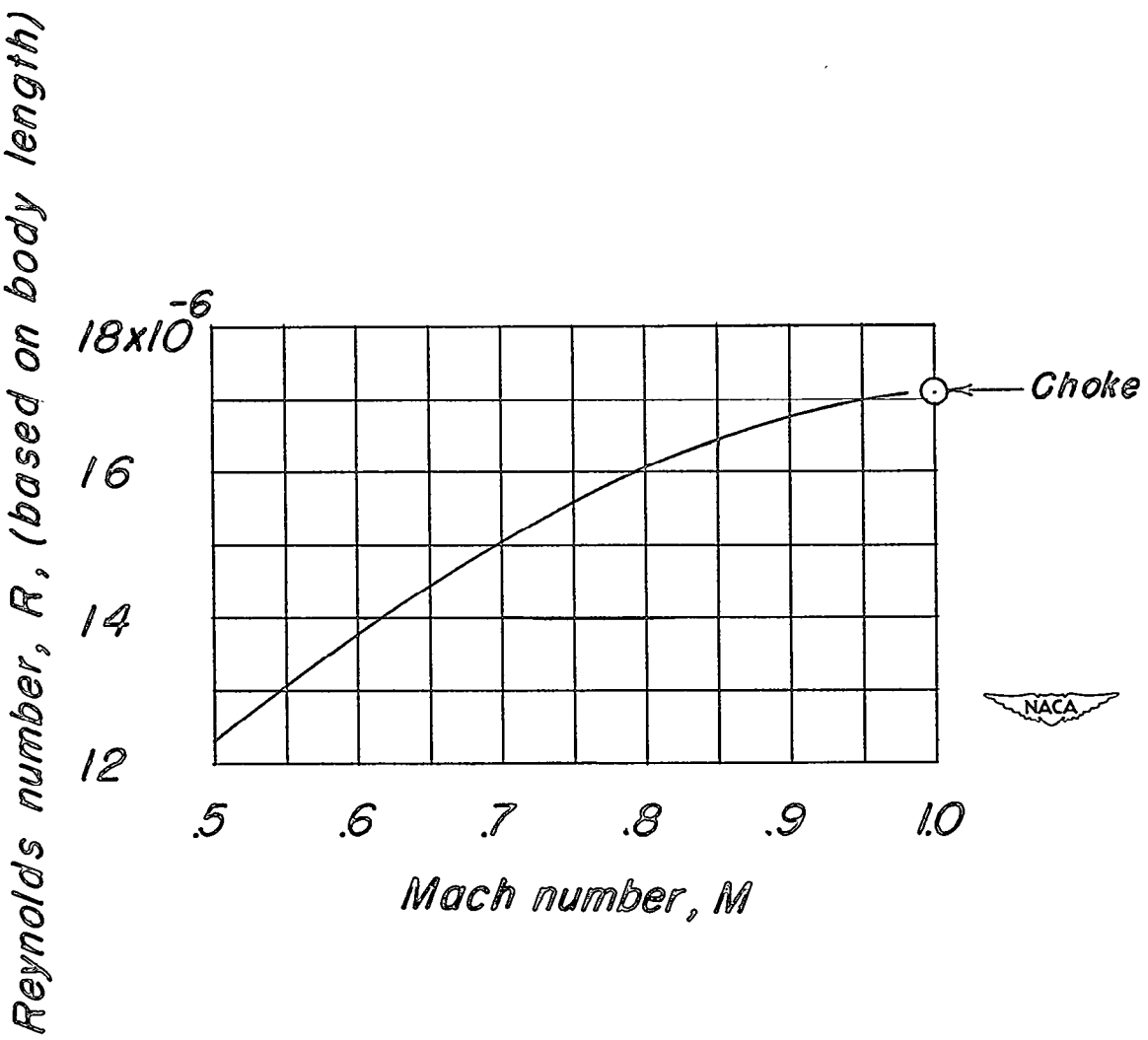

Figure 4.- Variation of test Reynolds number with Mach number for the test models.

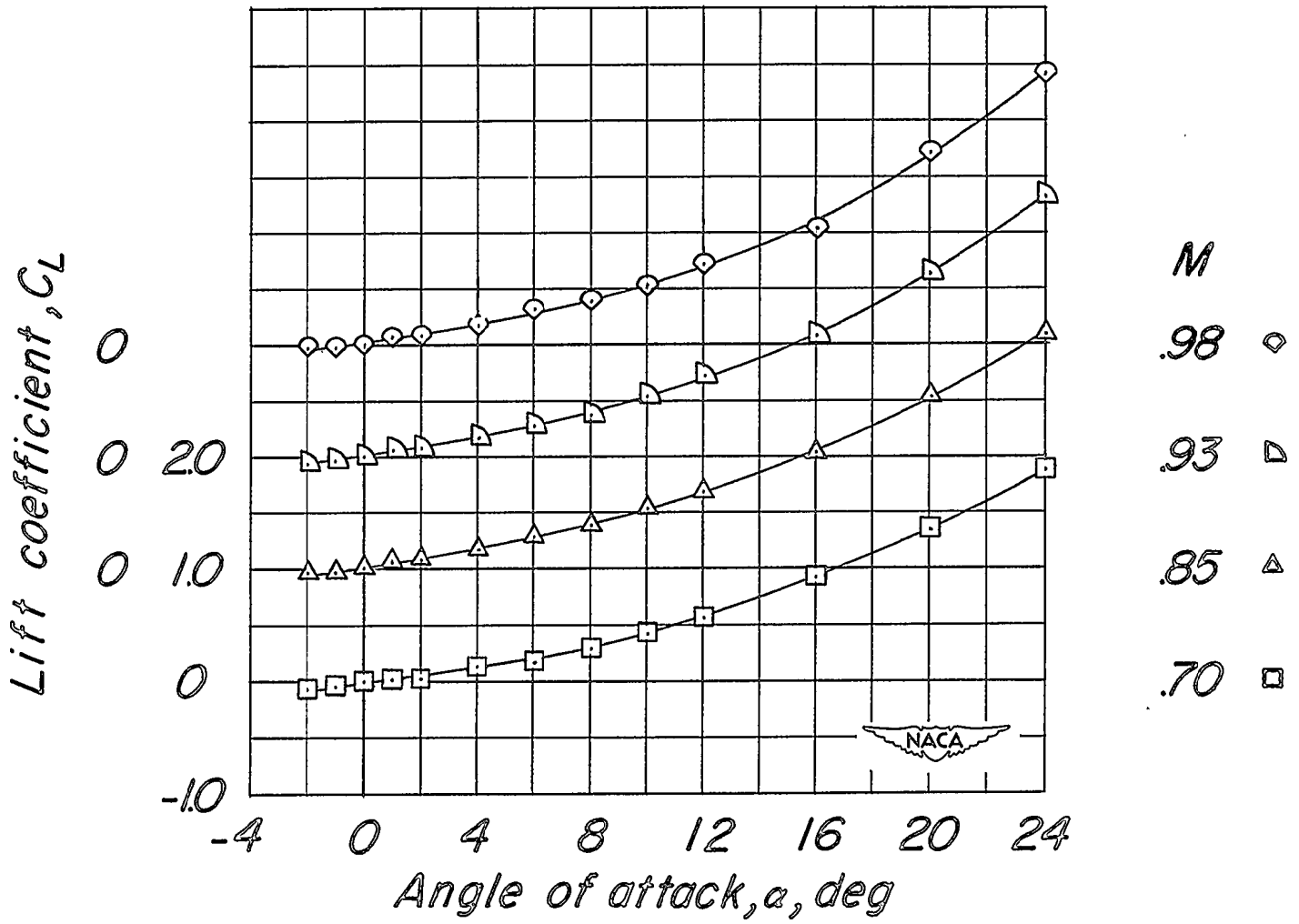

(a) C_L plotted against α.

Figure 5.- Aerodynamic characteristics of the body-alone configuration.

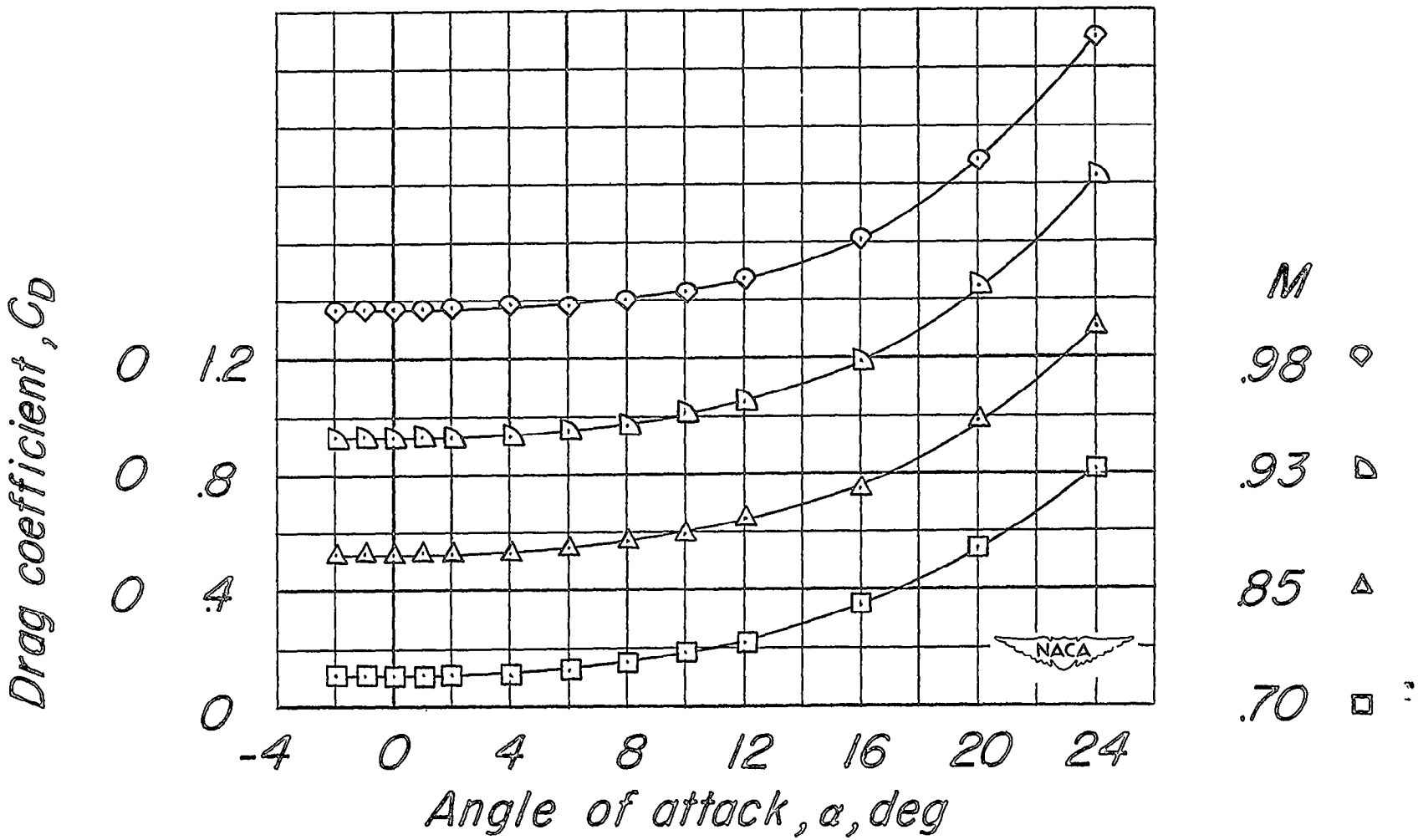

(b) C_D plotted against α.

Figure 5.- Continued.

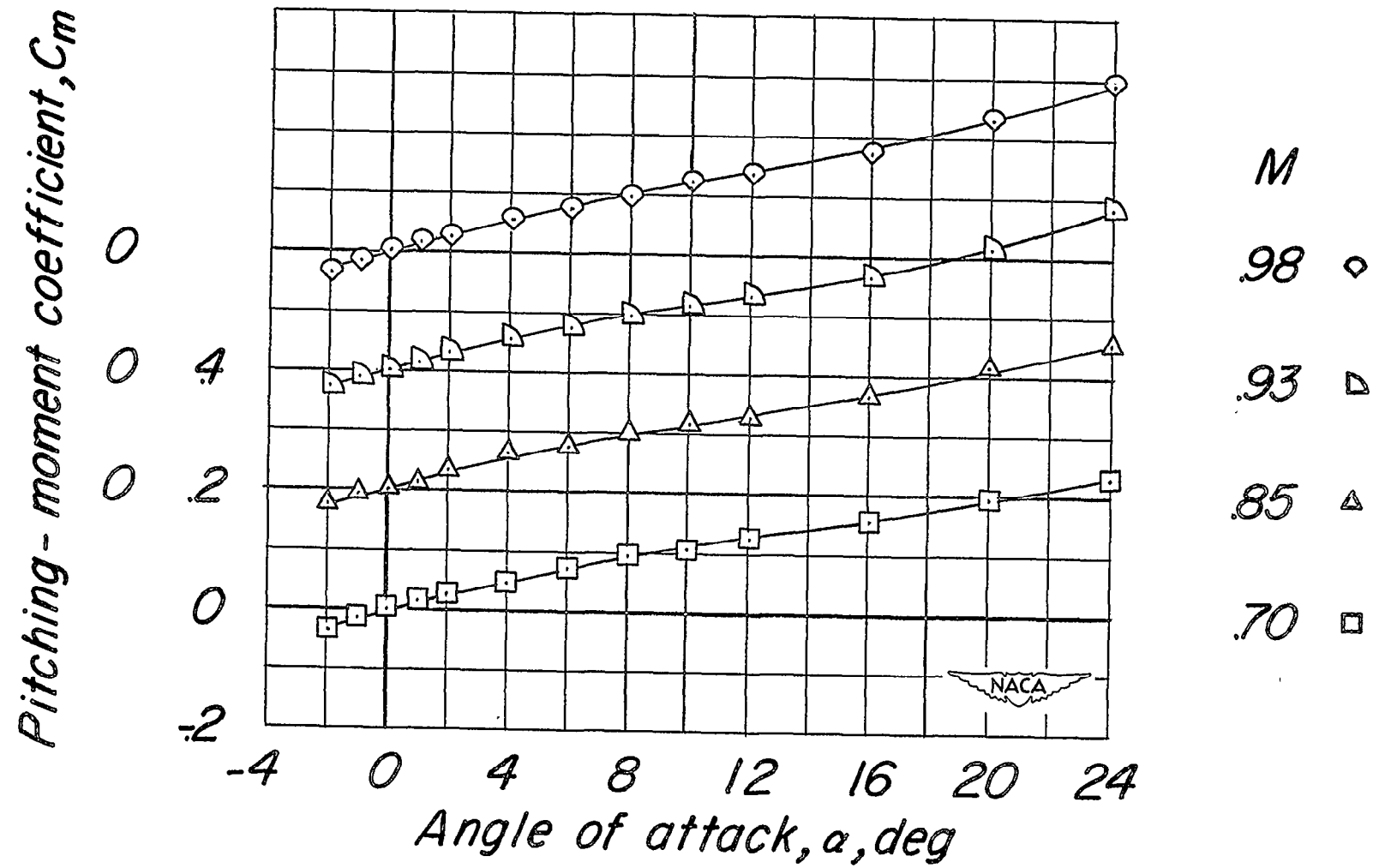

(c) C_m plotted against α.

Figure 5.- Concluded.

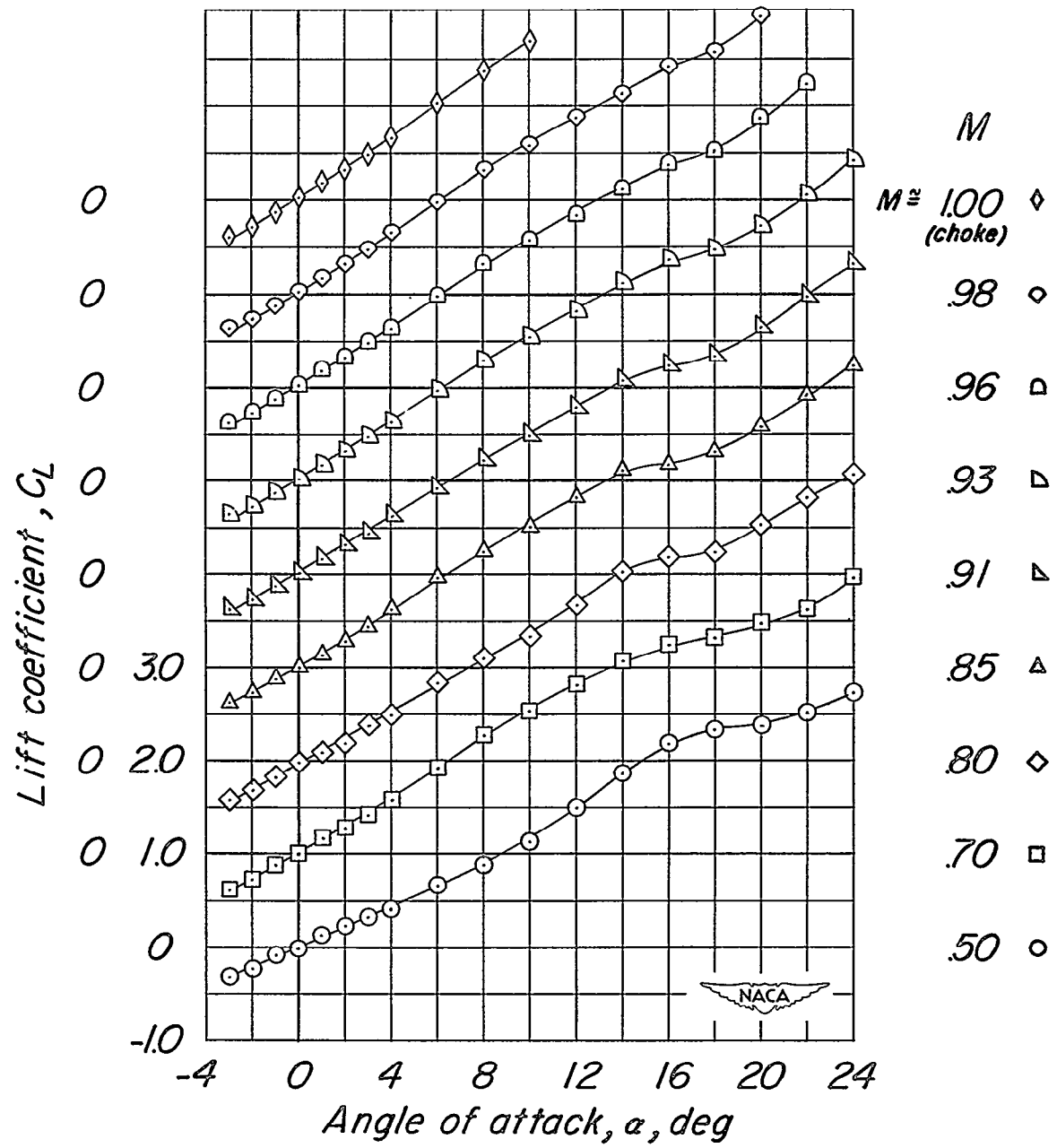

(a) C_L plotted against α.

Figure 6.- Aerodynamic characteristics of the body-fins combination, $\phi = 0^\circ$.

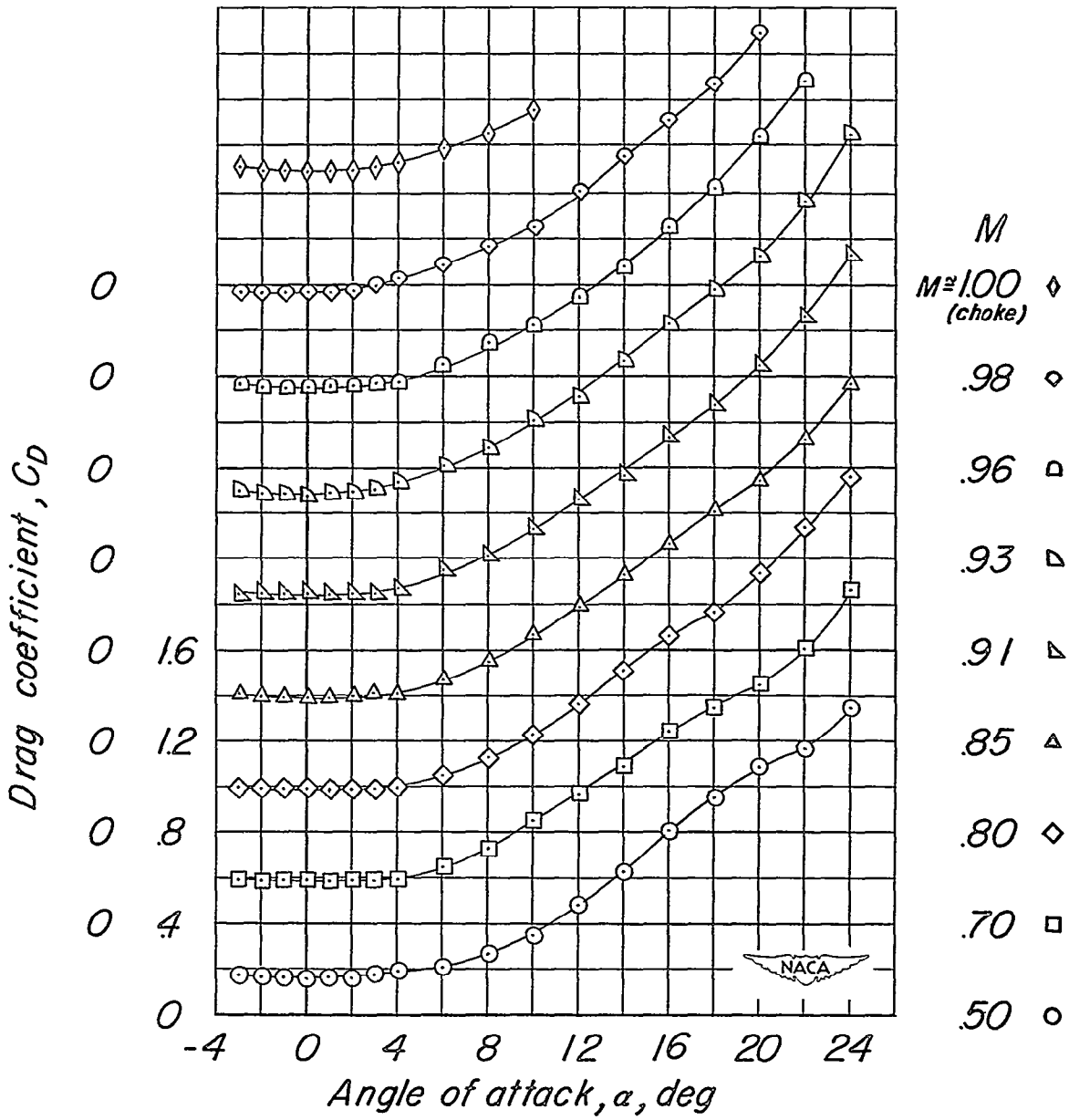

(b) C_D plotted against α.

Figure 6.- Continued.

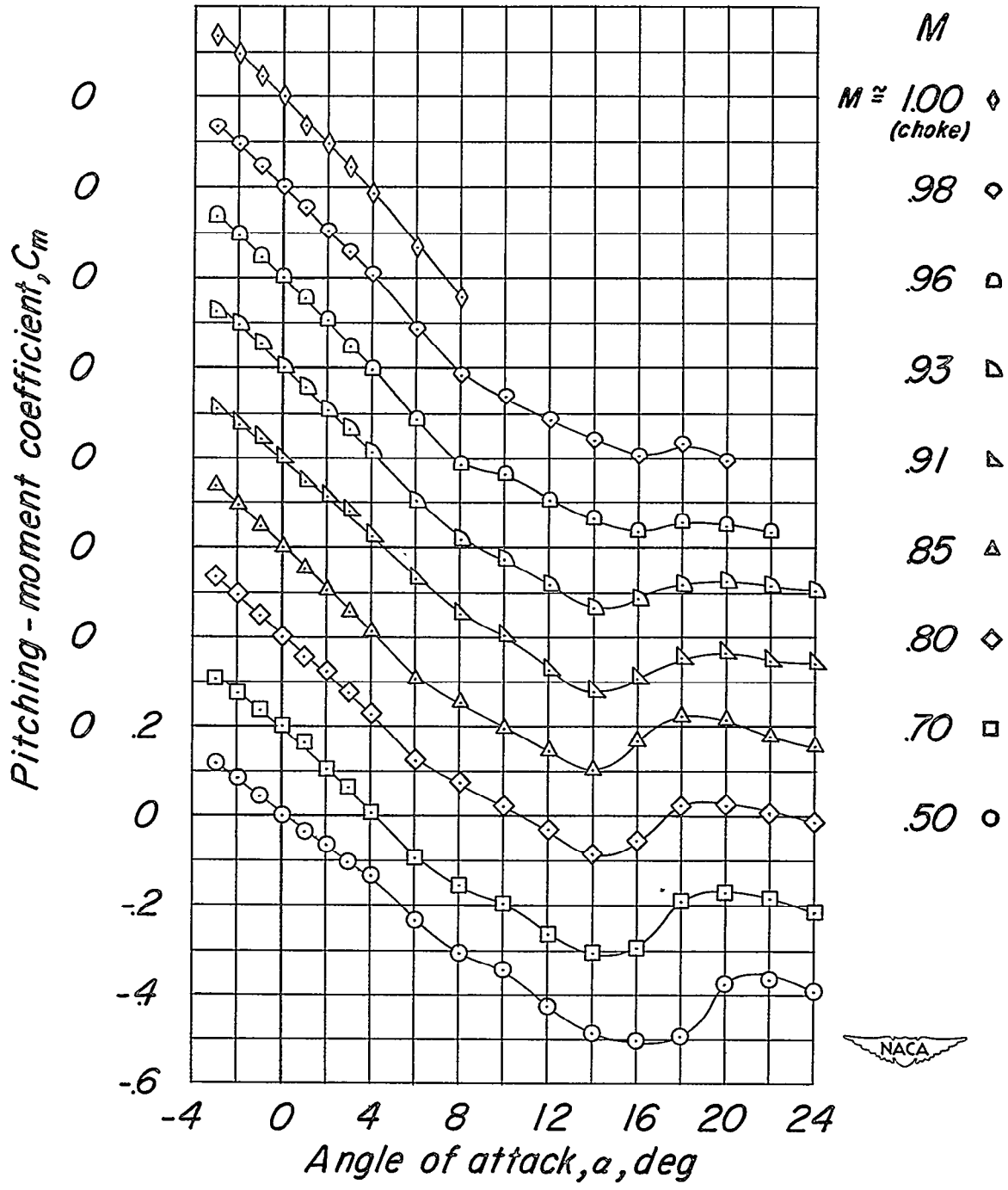

(c) C_m plotted against α.

Figure 6.- Concluded.

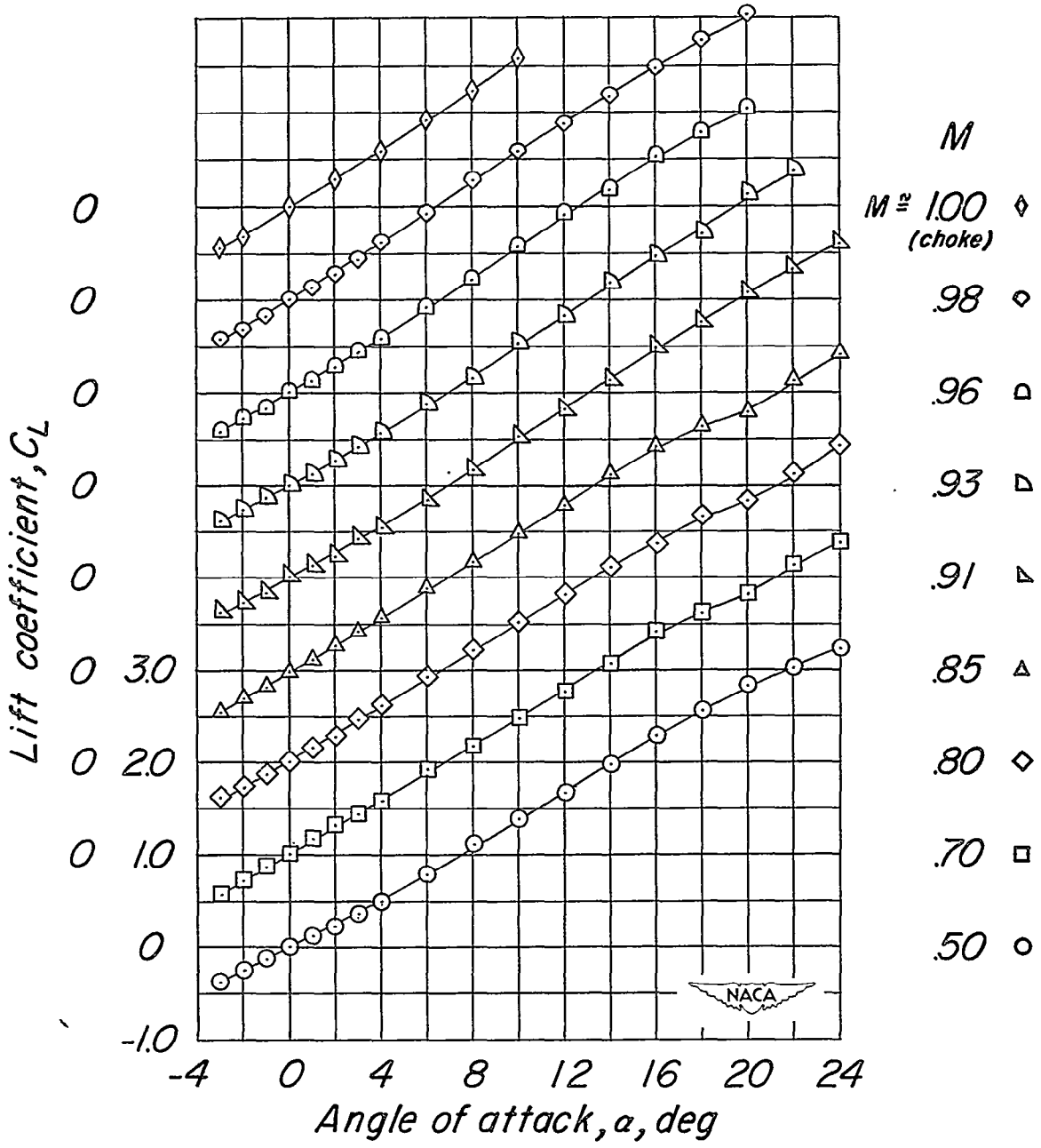

(a) C_L plotted against α.

Figure 7.- Aerodynamic characteristics of the body-fins combination, $\phi = 45^\circ$.

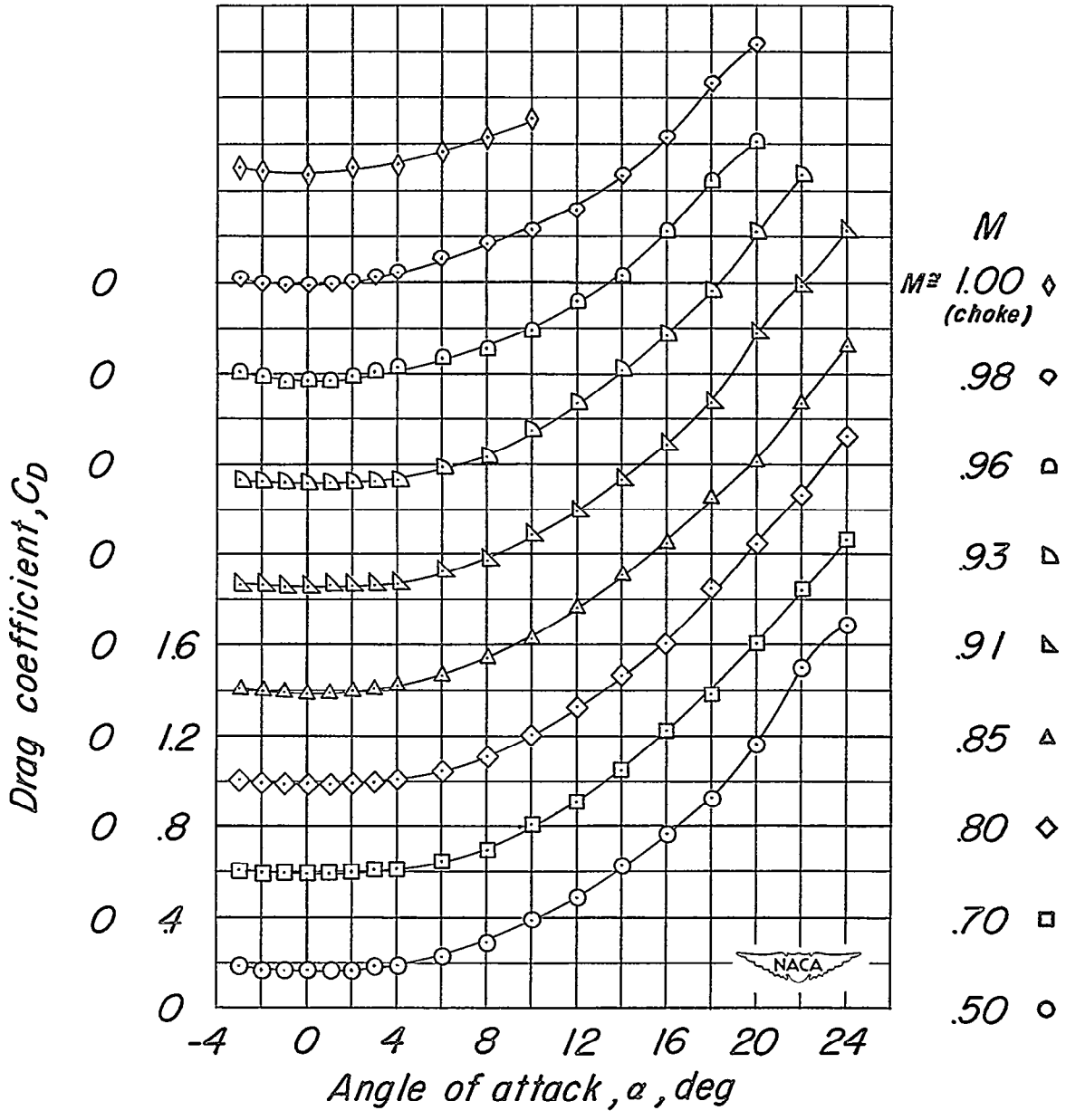

(b) C_D plotted against α.

Figure 7.- Continued.

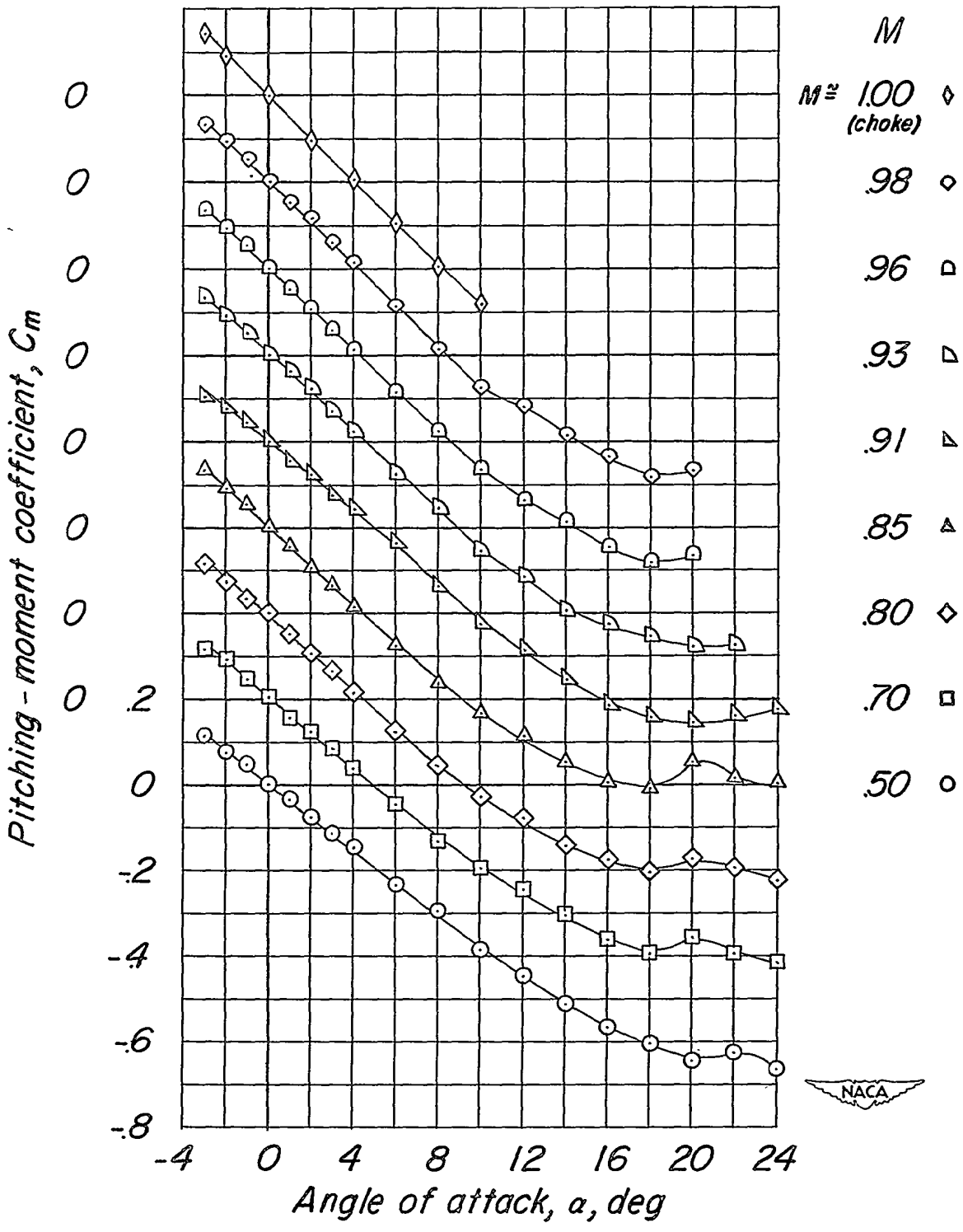

(c) C_m plotted against α.

Figure 7.- Concluded.

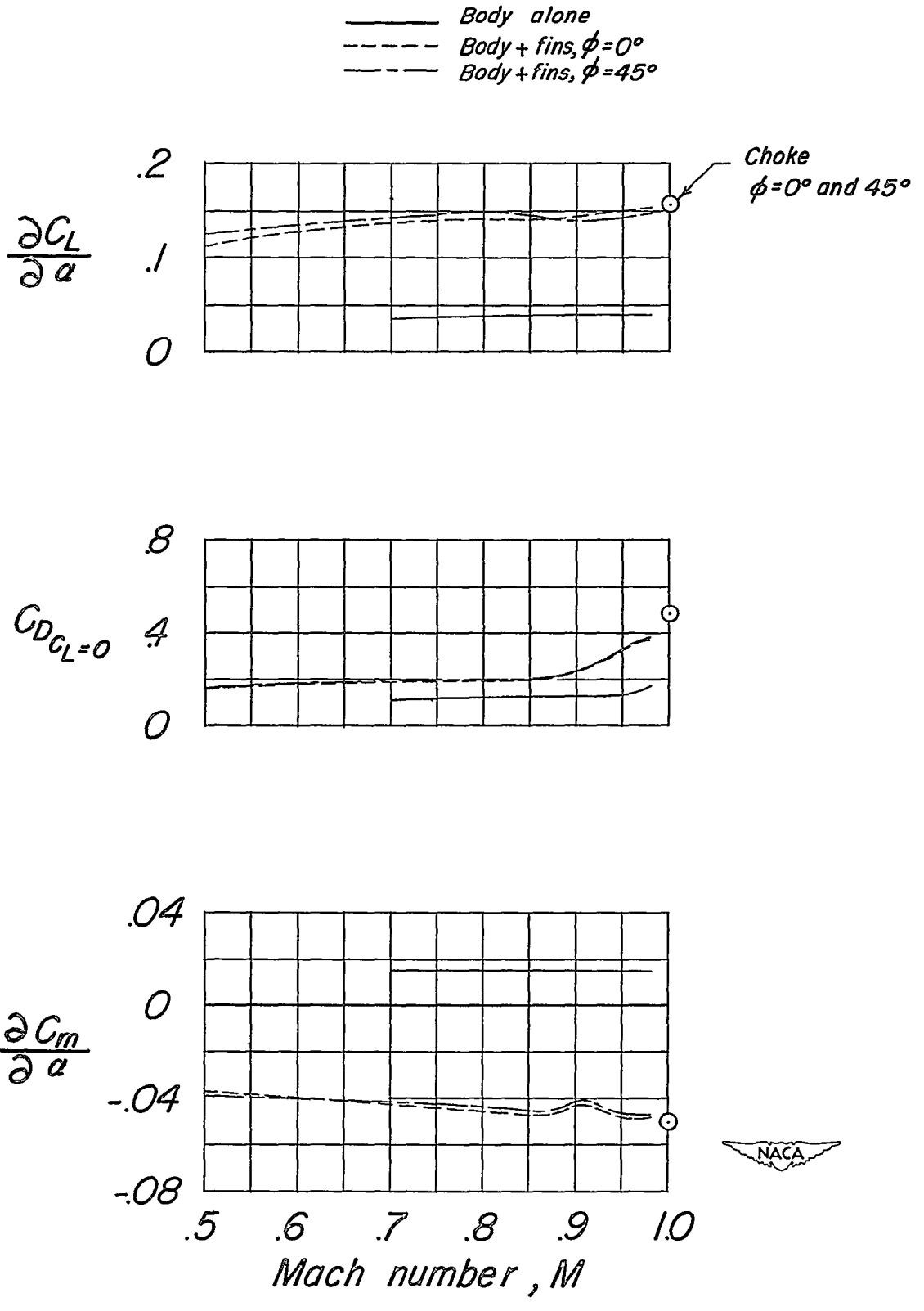

Figure 8.- Summary of the aerodynamic characteristics of the test models.

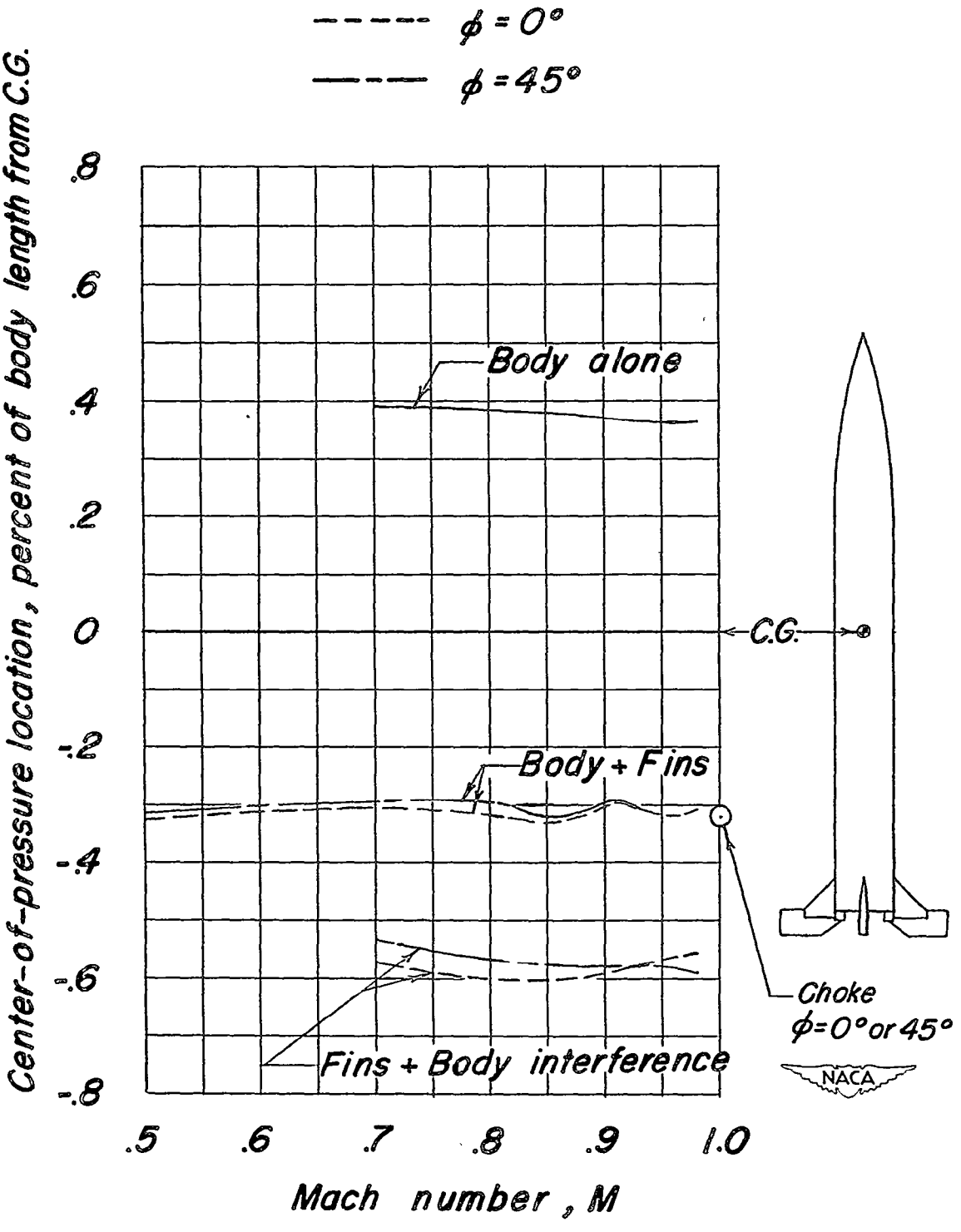

Figure 9.- Center-of-pressure locations of the test models.